Superconducting Magnetic Bearings (SMBs) for Turbo Molecular Pump Using High *Tc* Superconductors

K. Hara[1], M. Komori[1,*], N. Sakai[1], K. Asami[1], Y. Hanazawa[1]

[1]Department of Applied Science for Integrated System Engineering, Kyushu Institute of Technology,
1-1 Sensui, Tobata, Kitakyushu, Fukuoka 804-8550, Japan
*Corresponding Author: komori_mk@yahoo.co.jp, Tel. +81-93-884-3563, Fax. +81-93-884-3563

Abstract

This study was performed to apply superconducting magnetic bearings (SMBs) to a turbo molecular pump. First, we analyzed the system by using finite element method and design the structure whose vibrations are suppressed well. Then, we have made an experimental setup from the theoretical result. The experimental setup consists of two SMBs, a permanent magnet (PM) motor and a rotor with many turbine blades. We performed some experiments using this experimental setup in a vacuum chamber. In order to validate the theoretical result, some experimental tests have been carried out. In this paper, we discuss the dynamic characteristics of the spinning rotor with many turbine blades.

***Keywords**:* Cryogenic pump, Superconducting levitation, Magnetic bearing, High temperature superconductor, Turbo molecular pump

1. Introduction

Vacuum technology is necessary for the semiconductor industry, the medical industry and food industry [1]. The vacuum technology is also necessary for the new industry of space industry and other advanced industries [2]. Turbo molecular pumps are key technology for these industries. Turbo molecular pumps are usually composed of active magnetic bearings and its controllers [3]. Thus, the mechanism is very precise and complicated, which leads to high price. In this study, superconducting levitation techniques [4] are applied to turbo molecular pumps, because superconducting levitation is easy to use.

In this study, superconducting magnetic bearings (SMBs) [5] is used for a turbo molecular pump. Superconducting levitation force is produced by pinning effect between superconductors and PMs. The pinning effect means that magnetic flux is trapped in superconductor, which yield to levitation forces.

2. Design of Turbo Molecular Pump

2.1 Schematic illustration of setup

Fig. 1 shows an experimental setup image of turbo molecular pump. The experimental setup is

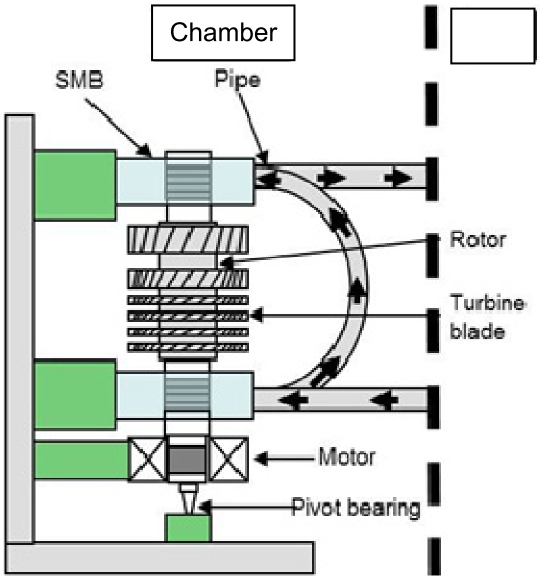

Fig. 1 Schematic illustration of the experimental setup image of turbo molecular pump

composed of a rotor with many turbine blades, two SMBs, a pivot bearing and a PM motor. The superconductors are cooled by using liquid nitrogen (-196 ^{o}C). Based on the experimental setup image, some experiments are performed in this study. The SMB is composed of a doughnut-shaped superconductor $Dy_1Ba_2Cu_3O_X$ (OD48× ID25.6× 15 mm, $J_c \approx 3 \times 10^8$ A/m^2 at 77 K and 1.0 T) and four PMs. The PMs are neodymium (Nd) magnets (OD24 mm ×W4.25 mm, surface magnetic flux density ≈0.26 T). The magnetic poles of the Nd PMs are arranged with alternate polarities, such as NS-SN-NS-SN.

In order to measure the dynamic characteristics of SMBs, a rotor with the two SMBs and without turbine blades is prepared. The rotor measures 232 mm in length and 24 mm in diameter. Then, impulse responses are measured by using the rotor. Fig. 2 shows an experimental result of impulse response for the rotor supported by the two SMBs. The result shows that the natural damped vibrations are

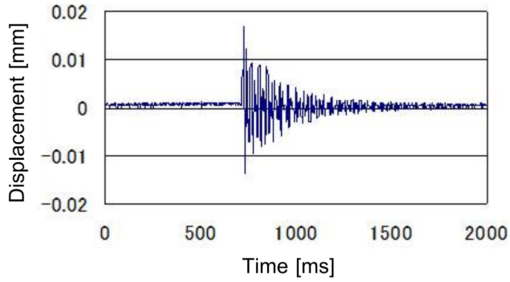

Fig. 2 Impulse response of the rotor supported by SMB

observed. The magnetic stiffness k =12,990 N/m and damping coefficient c =4.5 Ns/m are estimated. Hereafter, these values are applied to simulation parameters.

2.2 Rotor model

Fig. 3 shows the rotor models (model-1, 2, 3) supported by two kinds of bearings (SMB and pivot bearing). The rotor model-1 (Length: 192 mm), rotor model-2 (Length: 232 mm) and rotor model-3 (Length: 232 mm) are supported by (a) a SMB and a pivot bearing, (b) two SMBs and a pivot bearing, and (c) two SMBs. The rotor model-1, model-2 and model-3 measure 192 mm, 232 mm and 232 mm in length, respectively. Since these SMBs are the same as that used in Fig. 2, the magnetic stiffness k =12,990 N/m and damping coefficient c =4.5 Ns/m are applied to these models. The pivot bearing is composed of a small stainless bar (ϕ3 mm ×5 mm), which is attached to the rotor bottom.

By using the rotor models shown in Fig. 3, the rotor analysis (finite element method) is performed. The finite elements divided by many meshes are shown in Fig. 3. In the simulation, the rotor spins up to a speed of 20,000 rpm. Then, the displacements for three models are measured. Fig. 4 shows the simulation results of the relationship between rotor displacement and

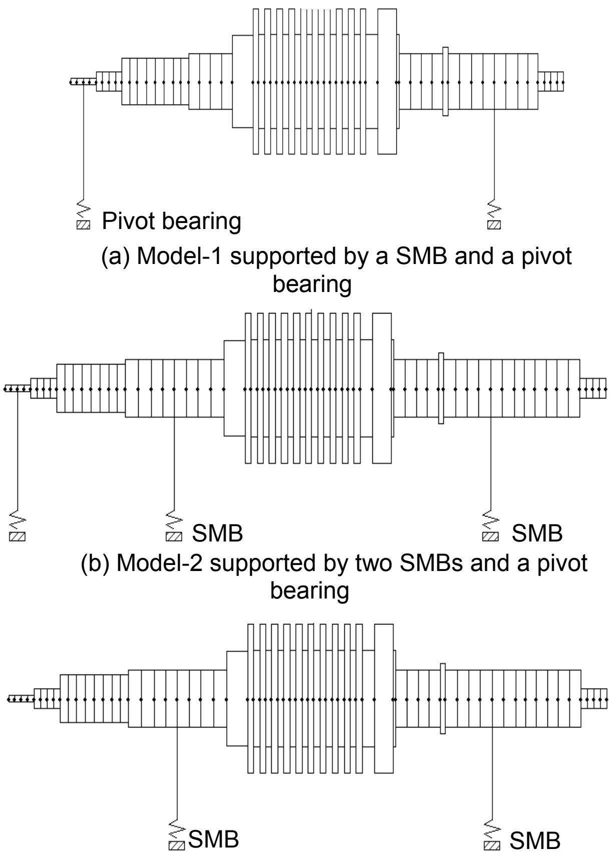

(a) Model-1 supported by a SMB and a pivot bearing

(b) Model-2 supported by two SMBs and a pivot bearing

Fig. 3 Rotor models supported by two kinds of bearings.

rotation speed for (a) the model-1, (b) the model-2 and (c) the model-3. The displacements in Fig. 4 (a) are analyzed near the points of pivot bearing, turbine blade and SMB. From the result in Fig. 4(a), each displacement is relatively small over a rotation speed range except for a speed of ≈5,000 rpm. Although the displacement near pivot bearing is almost zero at a speed of ≈5,000 rpm, the displacement peaks near turbine blades and near SMB are observed, which are caused by the bearing stiffness. The displacement is relatively very small over a wide range, because the ideal rotor has no distortion and no deformation. The displacements in Fig. 4(b) are analyzed near the points of pivot bearing, lower SMB, turbine blades and upper SMB. From the result in Fig. 4(b), each displacement is very small (smaller than 0.03 x10^{-3} mm) over a rotation speed range except for a speed range of ≈4,000 rpm. Although the displacement near pivot bearing is almost zero at a speed of ≈4,000 rpm, the displacement peaks near pivot bearing, lower SMB, turbine blades and upper SMB are observed. The displacements in Fig. 4(c) are analyzed near the points of lower rotor, lower SMB, turbine blades and upper SMB. From the result in Fig. 4(c), each displacement is very small (smaller than 0.02 x10^{-3} mm) over a rotation speed range except for a speed of ≈4,000 rpm. The displacement peaks near lower rotor, lower SMB, turbine blades and upper SMB are observed. And these peaks are almost the same value. This shows that rotor has a cylindrical

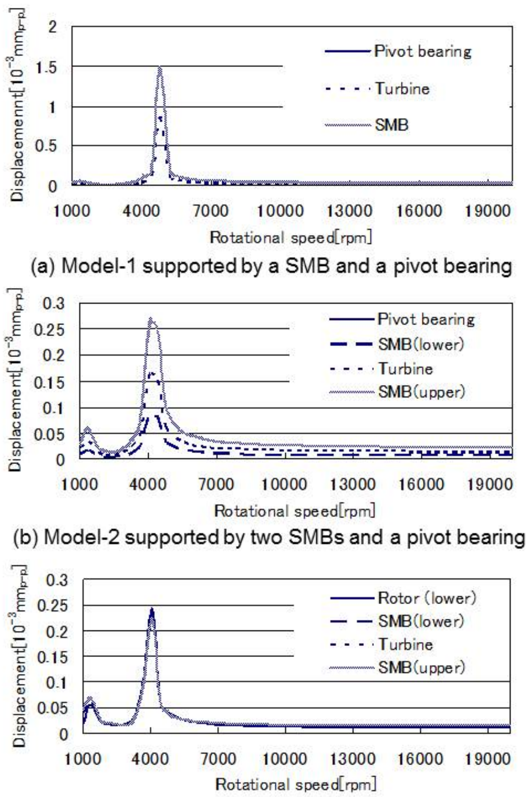

(a) Model-1 supported by a SMB and a pivot bearing

(b) Model-2 supported by two SMBs and a pivot bearing

(c) Model-3 supported by two SMBs

Fig. 4 Schematic results of rotor vibrations of three models 1-3.

motion at this rotation speed. Hereafter, the model-2 and model-3 are adopted in our study because of the small displacements, and the model-2 and model-3 are applied to some experiments.

3. Experiments and Discussions

The rotors are made according to the model-2 and model-3. Fig. 5 shows the schematic illustration of the developed rotor. The rotor is composed of turbine blades, PMs for SMB and a pivot for bearing. The turbine blades are a part of a real turbo molecular pump [6]. The PM is composed of four ring PMs (OD24 x 4.25 mm). The rotor is installed in the experimental setup as shown in Fig. 1. The SMBs are already explained in Fig. 1. The rotor model-2 and model-3 measure ≈590 g in weight.

Fig. 6 shows the experimental results of rotor displacements with two SMBs and a pivot bearing at speeds of (a) 1,000, (b) 4,000 and (c) 8,000 rpm. Upper displacement and lower displacement are measured in each figure. The upper displacement amplitudes at rotation speeds of (a) 1,000, (b) 4,000 and (c) 8,000 rpm are 0.06, 0.15 and 0.10 mm, respectively. The large upper displacement peak at a speed of 4,000 rpm is observed, which is corresponding to the large displacement peaks in Fig. 4(b). The lower displacement amplitude at each speed is almost the same as ≈0.06 mm. In the speed range higher than ≈8,000 rpm, the rotor stops the rotation because of large vibration displacements.

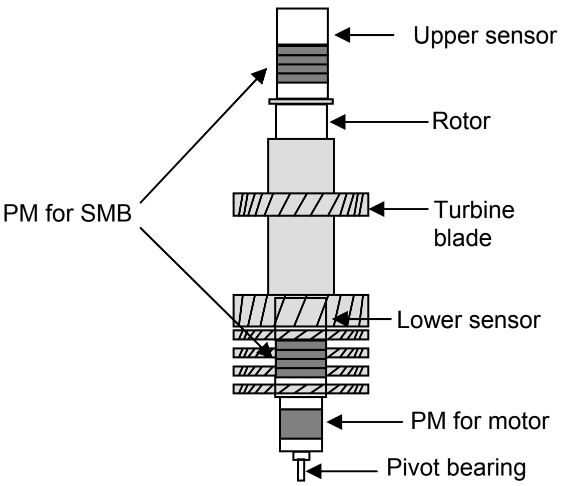

Fig. 5 Schematic illustration of the developed rotor

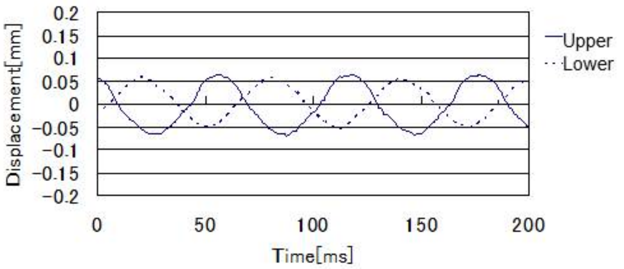

(a) 1,000 rpm

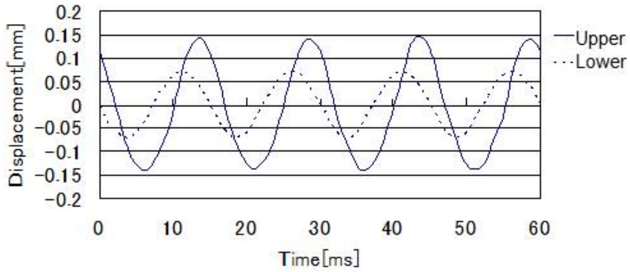

(b) 4,000 rpm

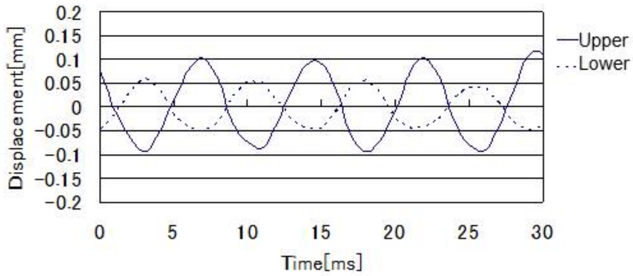

(c) 8,000 rpm

Fig. 7 shows the experimental results of rotor displacements with two SMBs at speeds of (a) 1,000, (b) 3,000, (c) 5,000, (d) 8,000 and (e) 20,000 rpm. Upper displacement and lower displacement are measured in each figure. The upper displacement amplitudes at speeds of (a) 1,000, (b) 3,000, (c) 5,000, (d) 8,000 and (e) 20,000 rpm are 0.04, 0.04, 0.09, 0.02 and 0.03 mm, respectively. The large upper displacement peak at a speed of 5,000 rpm is observed, which is corresponding to the large displacement peaks in Fig. 4(c). The upper displacement amplitudes in Figs. 7(a), (b), (d) and (e) (except for the resonance rotation speed) are a little smaller than the amplitudes shown in Figs. 6(a) and (c). The large upper displacement peak (0.09 mm) at the resonance rotation speed of 5,000 rpm in Fig. 7(c) is a little smaller than the upper peak (0.15 mm) at the speed of 4,000 rpm in Fig. 6(b). The lower displacement amplitude at each speed is almost the same as the upper displacement amplitude or smaller than that. From the experimental results in Figs. 6 and 7, the rotor (model-3) with two SMBs is better than the rotor (model-2) with two SMBs and a pivot bearing. This is because the larger displacement of rotor model-2 is caused by the pivot bearing. Hereafter, the rotor (model-3) with two SMBs is

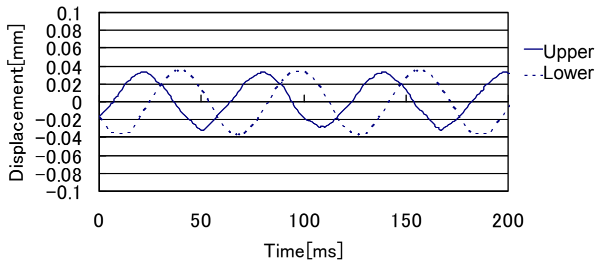

(a) 1,000 rpm

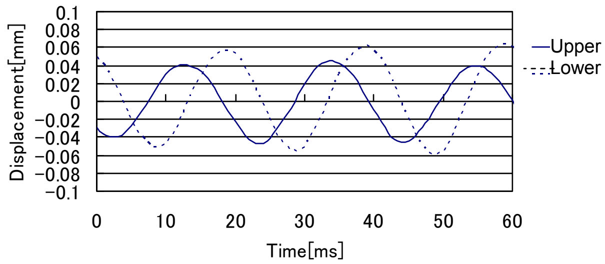

(b) 3,000 rpm

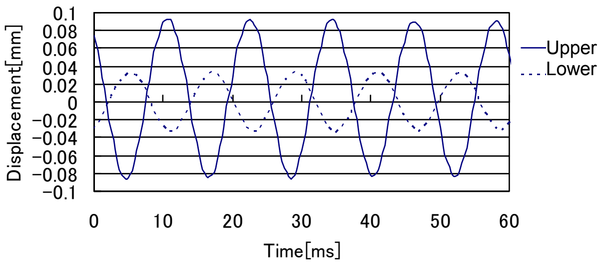

(c) 5,000 rpm

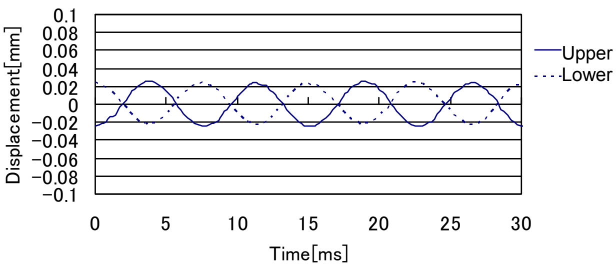

(d) 8,000 rpm

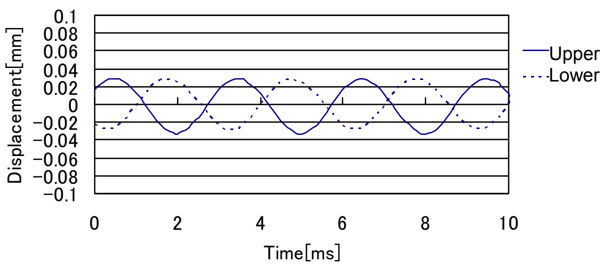

(e) 20,000 rpm

Fig. 7 Experimental results of rotor displacements with two SMBs

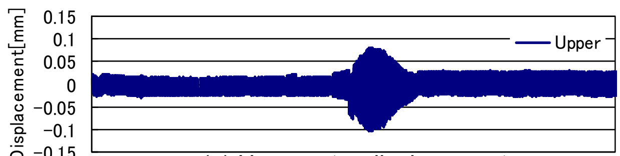

(a) Upper rotor displacement

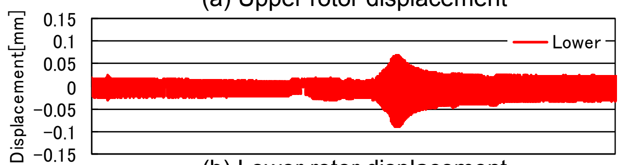

(b) Lower rotor displacement

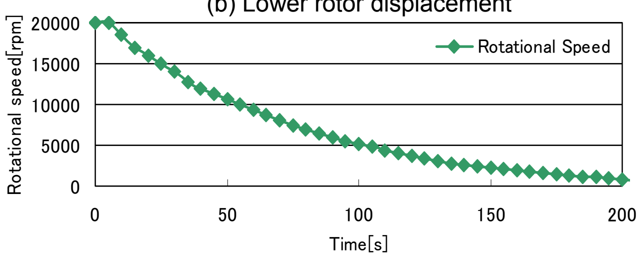

(c) Natural rotation decay curve

Fig. 8 Experimental results of free-run test for the rotor with two SMBs adopted in our study and some experimental tests are performed by using the model-3 rotor.

Fig. 8 shows the experimental results of free-run test for the rotor with two SMBs, showing (a) upper rotor displacement, (b) lower rotor displacement and (c) natural rotation decay curve. These results are corresponding to the results shown in Fig. 7. Figs. 8(a) and (b) show that the displacement amplitudes are smaller than 0.04 mm over a wide time range and large displacements at rotation speeds between ≈4,000 and ≈5,000 rpm are observed.

Fig. 9 shows a final image of turbo molecular pump with two SMBs. The rotor in Fig. 5 is installed in the molecular pump shown in Fig. 9. The molecular pump is composed of the rotor with two SMBs, turbine blades and a PM motor. The pump has a gas inlet at the top and a gas outlet at the lower side. Usually, the gas inlet is connected to a vacuum chamber using a vacuum hose. The pump exhausts the chamber to a certain degree of vacuum. At the same time, water molecules in the air are trapped on the

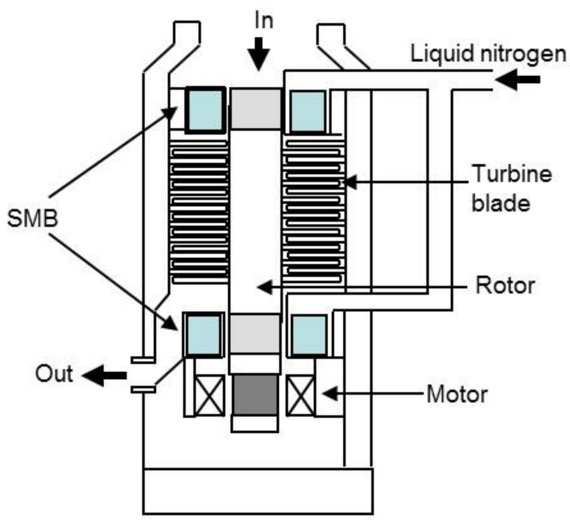

Fig. 9 Final image of turbo molecular pump

SMB surface and the turbine blades surface. This is called “trapping effect”. Then, such kinds of turbo molecular pumps with SMBs should evacuate chambers to a higher degree of vacuum than conventional turbo molecular pumps. Anyway, turbo molecular pumps shown in Fig. 9 have some higher performances than conventional turbo molecular pumps due to the trapping effect.

4. Summary

In this study, superconducting magnetic bearings (SMBs) is used for a turbo molecular pump. The rotor models (model-1, 2, 3) supported by two kinds of bearings (SMB and pivot bearing) are proposed. From the simulation results, the model-2 and model-3 are adopted from the three models because of the small displacements. From some experimental results for the rotor model-2 and model-3, it is found that the displacement amplitudes of the rotor model-3 are a little smaller than those of the rotor model-2 over a wide rotation speed range. This is because the larger displacement of rotor model-2 is caused by the pivot bearing. Finally, the model-3 rotor with two SMBs is adopted in our study and some rotation tests are performed by using this rotor.

5. References

[1] Weston, G. F. (1985). Ultrahigh vacuum practice, Butterworths.

[2] Jayaram, S., and Gonzalez, E. (2011). Design and construction of a low-cost economical thermal vacuum chamber for spacecraft environmental testing, Journal of Engineering,

Design and Technology, vol. 9 (1), 2011, pp.47 – 62.

[3] Japan Society of Mechanical Engineering, Active magnetic bearing and the application, Yokendo Co. Ltd.

[4] Moon, F. C. and Chang P. -Z. (1990). High-speed rotation of magnets on high Tc superconducting bearings, Applied Physics Letter, vol. 56, 1990, pp. 397-399.

[5] Komori, M. and Kitamura, T. (1992). Superconducting bearing using high-Tc superconductors for potential applications, Procs. of the 3rd International Symposium on Magnetic Bearings, Alexandria, USA.

[6] Pfeiffer Balzers Turbo Pump, TPH-060, URL: http://www.pfeiffer-balzers.com